ADVANCED MATERIALS TECHNOLOGIES
www.advmattechnol.de

Fully Printed Flexible Ultrasound Transducer for Medical Applications

*Kirill Keller, Christoph Leitner, Christian Baumgartner, Luca Benini, and Francesco Greco**

The fabrication of a fully printed, lead-free, polymer piezoelectric transducer is presented and the characterization of its structural, dielectric, and ferroelectric properties at different processing stages is demonstrated. The performance of poly(vinylidene fluoride-trifluoroethylene) transducers with resonance frequency analyses, acoustic power measurements, and pulse-echo experiments is evaluated. Notably, for the first time for a fully printed transducer, an optimal performance in the medical ultrasound range (<15 MHz) is demonstrated with acoustic power >1 W cm^{-2}, which is promising for applications in epidermal and wearable electronics. Overall, the findings provide a strong foundation for future research in the area of flexible ultrasound transducers.

1. Introduction

Ultrasound (US) devices play a crucial role in medical imaging and diagnosis.[1] The non-ionizing nature and high penetrating capability of US devices make them an ideal tool for safe, noninvasive, and prolonged examination of human tissues. In medical pulse-echo US short acoustic pulses with frequencies of typically 2–15 MHz are generated and sent into the body.[2] Their reflections from internal structures are in turn recorded with the same probe. In this manner, the structure and morphology of the examined tissue and its functionality can be assessed. The main element of modern commercial US probes is a piezoceramic transducer, which is intrinsically rigid, stiff, and suffers from a high mechanical and acoustic impedance mismatch with human tissues.[3] As a result, commercial probes do not flex and conform to the human anatomy and they require the application of ultrasound gel which dries over time, limiting the long-term measurements. The gel can leave a greasy residue on the skin, cause skin drying, general discomfort for the patient or even allergic reactions.[4] Moreover, commercial probes employ additional matching and backing layers, leading to increased complexity and bulkiness. On the other hand, backend acquisition hardware used in commercial setups also has many constraints. Existing research systems are heavy and unwieldy, while mobile handheld systems are lightweight but suffer from limitations in high frame-rate data processing.[5] Therefore, wearability of US is a two-end open problem, which has been subject of intense recent research.

K. Keller, F. Greco
Institute of Solid State Physics
NAWI Graz
Graz University of Technology
Petersgasse 16, Graz 8010, Austria
E-mail: francesco.greco@santannapisa.it

C. Leitner, L. Benini
Integrated Systems Laboratory
ETH Zurich
Gloriastrasse 35, Zurich 8090, Switzerland

C. Baumgartner
Institute of Health Care Engineering with European Testing Center of Medical Devices
Graz University of Technology
Stremayrgasse 16, Graz 8010, Austria

L. Benini
Department of Electrical
Electronic and Information Engineering "Guglielmo Marconi"
University of Bologna
Via Zamboni 33, Bologna 40126, Italy

F. Greco
The Biorobotics Institute
Sant'Anna School of Advanced Studies
Viale R. Piaggio 34, Pontedera 56025, Italy

F. Greco
Department of Excellence in Robotics and AI
Sant'Anna School of Advanced Studies
P.zza Martiri della Libertà, Pisa 56127, Italy

The ORCID identification number(s) for the author(s) of this article can be found under https://doi.org/10.1002/admt.202300577

DOI: 10.1002/admt.202300577

Recently, US acquisition hardware has started to undergo a transformation to enable truly wearable applications. In contrast to conventional medical systems, wearable US devices should enable wireless data transmission of multiple channels over a period of several hours of continuous and unobtrusive monitoring during human movement without impairing range of motion.[6–8] These advancements have expanded the potential of US technology to new application areas, which were previously impossible to envision with larger, bulkier systems.[6,9,10]

On the other hand, piezoelectric US transducers have experienced an impetus due to the development of thin-film technology and its integration into skin-adherent hydrogel,[9] or elastomer matrix.[11] The incorporation of lead zirconate titanate (PZT) piezoelectric elements within more pliable carriers has resulted in a significantly improved wearability of transducers. However, these probes are made exclusively from lead-containing ceramics.[12] These have excellent piezoelectric properties, but their fabrication is complex and expensive. Moreover, high processing temperatures and aggressive chemical environments are required. In addition, a high degree of acoustic impedance mismatch between the PZT and human tissue necessitates the inclusion of additional substructures, further intricating the fabrication of layer stacks.

Conversely, there has been increasing interest in alternatives to conventional piezoceramic transducers based on (bio)polymers.[13–15] Polymer-based capacitive micromachined US transducers (polyCMUT), for example, are an emerging technology offering wider bandwidth than most ceramics, fast fabrication processes and a high degree of integration.[16,17] Despite their potential advantages, the need for constant DC bias voltage, as well as limited sensitivity and power delivery can pose design and application challenges.[18]

Another potential lead-free alternative to conventional piezoelectric ceramics is the use of softer piezoelectric polymers.[19] Polyvinylidene fluoride (PVDF) and its copolymers have several advantages compared to piezoceramics: their processing requires lower temperatures (typically below 150 °C, compared to above 1000 °C for piezoceramics)[20] and it is compatible with solution-based deposition methods, such as several printing and additive manufacturing techniques. Despite its weaker electromechanical coupling characteristics, PVDF offers all the advantages of a typical polymer, both in terms of its chemical tailorability and functionalization as well as for its reduced stiffness, leading to improved flexibility and conformability, as required for wearables. In addition, PVDF has an acoustic impedance (1.6–6 MRayl)[21,22] similar to that of human tissue (1.5 MRayl),[23] eliminating the need for additional matching layers.

The unique properties of PVDF and its copolymers make them suitable for use in various applications, such as nanogenerators, pressure, strain, vibration sensors, etc.[24–27] Despite these benefits, most research and development efforts have been directed toward the creation of receiver (able to sense and receive incoming signal) transducer elements, while the fabrication of transmitting (able to generate acoustic waves) elements remains a challenge. Among other factors, the thickness of the PVDF layer determines the resonance frequency of its oscillations.[28]

For example, a freestanding PVDF transducer with a film thickness of 50 μm will resonate at 48 MHz. Every additional structure added to the transducer (e.g. electroding, backing, matching, etc.) will affect the resonance behavior.[29] In case of a low impedance backing such as air, for example, the transducer will begin to oscillate in its $\lambda/2$ mode, causing harmonics occurring at 24 MHz, 48 MHz, and so on.[21] Adding additional substructures, e.g., printing substrates, can further affect the resonance behavior depending on their acoustic impedance and thickness, and cause oscillations also in the $\lambda/4$-mode. In printed flexible electronics, soft polymer substrates with similar acoustic impedances to PVDF such as PI, PEN, PET or PDMS are typically used.[30] Hence, not only the active piezoelectric layers, but also passive substrates can be utilized to modulate the frequency band of transducers, by carefully adjusting their thickness. Thus, depending on the type and thickness of the substrate, additional harmonic peaks may be generated allowing for harmonics in the medical frequency range.[31,32] Al Mohimeed et al., for example, have used these principles for the optimization of their thin-film poly(vinylidene fluoride-trifluoroethylene) (P(VDF-TrFE)) transducers.[33] However, manual thin-film assembly requires additional adhesive layers to adhere substructures and can cause backreflection and poor reproducibility. The use of printing methods can overcome the latter. Although there have been examples of fully printed transmitting ultrasound transducers operating in the high-frequency range (≈100 MHz),[34] no fully printed PVDF-based US transducers that operate in the medical frequency range have been reported.

Within this context our work demonstrates a fully printed single-channel flexible US transducer. We employ a combination of inkjet and screen printing methods to fabricate the transducers in a fast, customizable, and cost-efficient manner. The probes are able to resonate at frequencies in the bandwidth of conventional medical ultrasound systems and can be used both as a US transmitter and receiver. We achieved an acoustic power >1 W cm^{-2} at a frequency $f = 13.6 \pm 0.6$ MHz, which is comparable with the performance of conventional PZT transducers.[35]

Figure 1 provides a visual overview and summary of our study. We show the fabrication recipe for our samples and feature a comprehensive analysis of the transducer properties. Specifically, we provide details on the characterization process and emphasize significant experimental outcomes, such as acoustic power and resonance frequencies. The operation of printed US transducers is validated in a pulse-echo experiment. We demonstrate that transducers are capable of transmitting and receiving acoustic waves in the targeted medical frequency range.

2. Experimental Section

2.1. Fabrication of Printed US Transducer

The fabrication process of P(VDF-TrFE) US transducers was performed in three steps:

1) inkjet printing of Ag bottom electrode,
2) screen printing of P(VDF-TrFE) layers on top of bottom electrodes, and
3) inkjet printing of Ag top electrode.

As a flexible printing substrate a polyimide (PI) sheet with a thickness of 50 μm (Kapton HN DuPont, USA) was used. Before printing, the PI substrate was treated with oxygen plasma

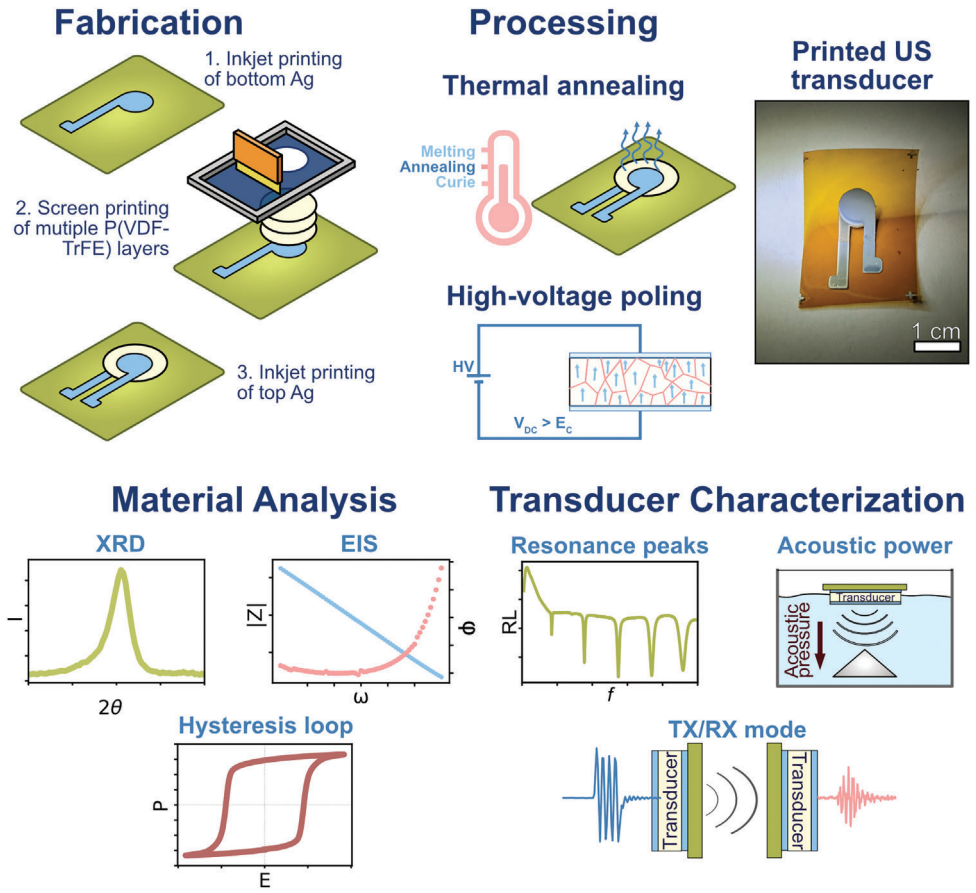

Figure 1. Schematics of the study. Top: illustration of the fabrication and applied processing of the printed US transducer. Bottom: methods used to characterize the effect of the processing on materials properties of P(VDF-TrFE) and performance of the printed transducer.

(t = 10 s, power 40%, pressure 0.3 mbar; carried out with a 40 kHz 100 W, Diener Femto Plasma Cleaner, Germany) in order to clean the surface and improve the wettability. Ag electrodes were fabricated on PI by ink-jet printing of a reactive silver ink (EI-710 from Electroninks, USA) with a Dimatix Materials Printer (DMP-2850, Fujifilm, USA) equipped with cartridges having a nominal drop volume of 10 pL. Circular electrodes (⌀ 8.5 mm) were printed with a drop spacing of 15 µm and the substrate table was set to a temperature of 60 °C at which the organic silver complexes start to decompose into metallic silver. After printing electrodes, they were annealed in the oven at T = 100 °C for 10 min in order to remove the residual solvents. The thickness of the Ag electrodes was ≈500 nm, as determined by stylus profilometry (see details below).

The poly(vinylidene fluoride-trifluoroethylene) (P(VDF-TrFE)) ink was formulated similarly to previously published procedures.[36] Piezotech FC20 (purchased from Arkema, France) is a P(VDF-TrFE) powder with a content of TrFE of 20 mol%. P(VDF-TrFE) was dissolved in a mixture of methyl ethyl ketone and dimethyl formamide with a weight ratio 1:9 producing a 20 wt% of P(VDF-TrFE) solution.[37] The ink was sonicated in an ultrasonic bath for at least 30 min to eliminate air microbubbles, before using it for printing. Layers of P(VDF-TrFE) were printed with a custom manual screen printing press equipped with a self-prepared 77 threads cm^{-1} mesh screen. Screens were designed with a pattern comprising an array of 4 circles (⌀ 15 mm). Each layer was dried on a heating plate at T = 60 °C for 3–5 min before printing the next layer. After deposition of the last layer and before printing the top electrode, the samples were placed in an oven at T = 100 °C for 10 min in order to remove the rest of the solvents. The total thickness of a transducer depended on the total number of printed layers (in this study the number of printed layers varied from 6 to 12). Afterward, the top Ag electrode was inkjet printed according to the same procedure described above for the bottom one. Finally, transducers were thermally annealed in an oven at T = 140 °C for 60 min. The active surface of transducers is circular and has a diameter of 8.5 mm.

2.2. Poling Procedure

Printed US transducers were polarized in a contact poling procedure at room temperature[38] during 10 cycles (sequence per each cycle: 25 s high-voltage application, 10 s rest, 25 s high-voltage application with reversed polarity, 10 s rest) using an in-house custom bipolar DC high-voltage generator (**Figure 2**a). At each cycle the voltage was gradually increased until the applied field reached an average of $E = 1.5\ E_{C,}$ being E_C the coercive field

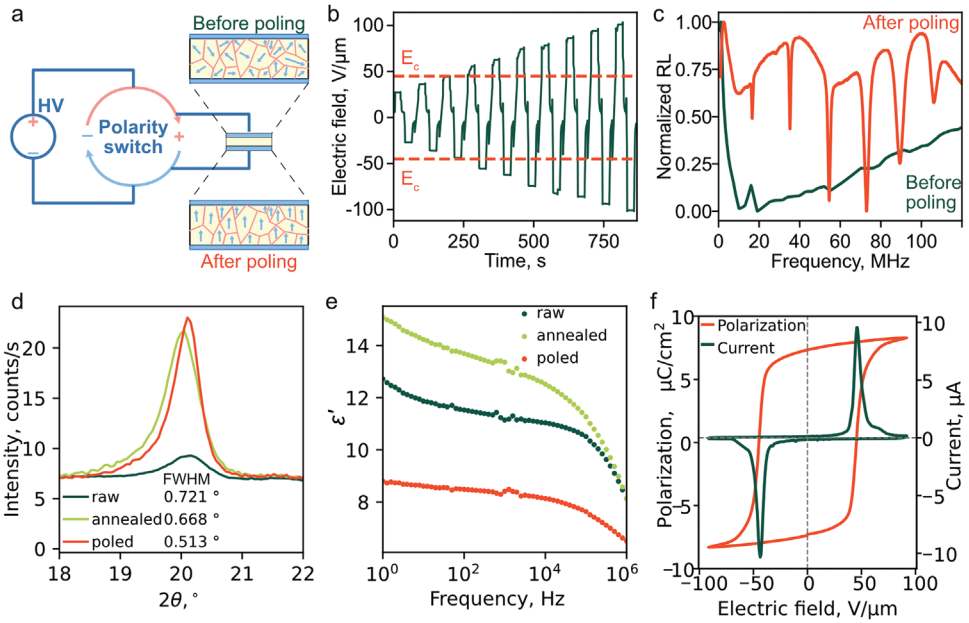

Figure 2.. a) Schematics of the in-house built high-voltage poling setup. b) The applied cycles of poling electric field over time, with the gradually increasing electric field, well over the coercive field $E_c = 45$ V μm^{-1}. c) Frequency versus normalized return loss (RL) of a printed transducer before and after poling. d) X-ray diffractogram and e) relative permittivity as a function of frequency of printed transducer after printing ("raw"), thermal annealing ("annealed"), and poling ("poled"). f) *P*–*E* hysteresis loop of a poled sample, showing the remnant polarization P_r and coercive field E_c.

($E_C = 45$ V μm^{-1} for FC20)[39] (a typical poling sequence is shown in **Figure 3**b).

2.3. Dielectric and Piezoelectric Characterization

The impedance of printed US transducers was measured with the Gamry Reference 600 potentiostat (Gamry Instruments, USA) in 2-electrode configuration, in the frequency range of 1 Hz–1 MHz with an applied AC voltage of 1 V. For XRD measurements the transducer with 12 μm thick P(VDF-TrFE) layer was attached to a Si wafer with a biadhesive tape. The XRD was measured in the range of $2\theta = 6°$–$50°$ with a Panalytical Empyrean diffractometer (PANalytical, the Netherlands, Cu tube, $\lambda = 1.5418$ Å). Hysteresis loops of piezoelectric transducers indicate the polarization (*P*) at the applied electric field (*E*). Three *P*–*E* loops were recorded on each of the five samples with the AIXPES Piezoelectric Evaluation System (AixACCT, Germany) at 0.1 Hz. The remnant polarization (P_r) was identified at zero electric field and the coercive field (E_C) was determined at zero net polarization.

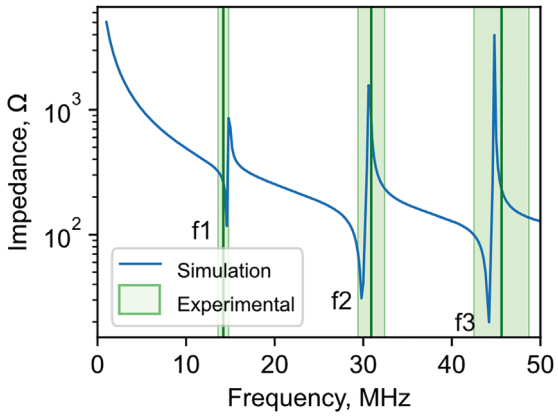

Figure 3. Resonance behavior of printed US transducers (with a 24 μm thick active layer of P(VDF-TrFE) on a 50 μm thick PI substrate): simulated frequency spectrum of printed US transducer, superimposed with experimental frequency ranges corresponding to the resonance peaks (shaded area represents one standard deviation).

2.4. Thickness Measurements

Single layers of P(VDF-TrFE) and Ag (five samples each) were deposited separately on a Si wafer. Thicknesses of these printed materials were measured with a stylus profilometer KLA-Tencor D-500 (KLA, USA). Since the piezoelectric elements consist of up to 12 layers of P(VDF-TrFE) their total thickness was calculated by multiplying the thickness of a single layer by the number of deposited layers.

2.5. Resonance Behavior of Printed US Transducers

Resonance behavior of printed US transducers was evaluated by measuring the return losses during a frequency sweep in the range of 1–120 MHz with a vector network analyzer (VNA) miniVNATiny (mini Radio Solutions, Poland). Transducer electrodes were contacted via a custom sample holder. VNA signals were transferred via an SMA connector to a custom printed circuit board (Figure S1, Supporting Information). This board interfaces the device under test using spring loaded Pogo pins. This allows good electrode contacts on the flexible samples, a short

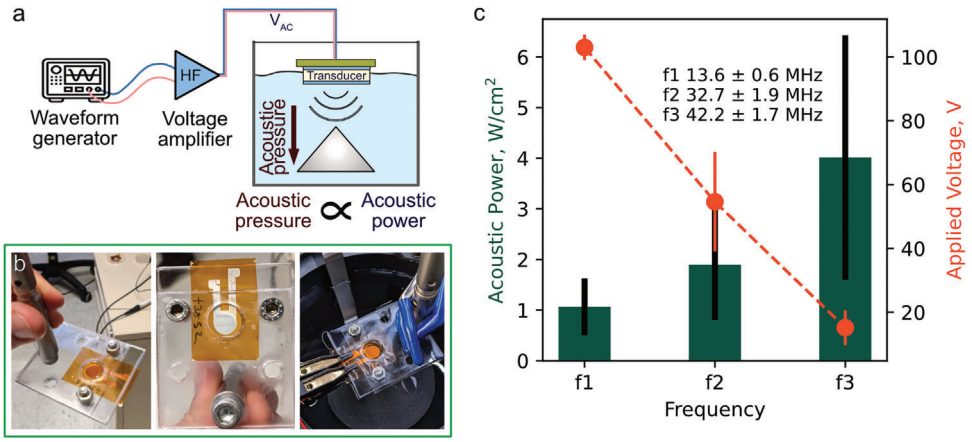

Figure 4. Acoustic power measurements of printed US transducers. a) Schematics of the acoustic power measurement set-up with the printed US transducers partially immersed (face down) in a water tank. b) Photos of the transducer in a sample holder from top, bottom, and fixed on the surface of the water. c) Acoustic power and applied voltage at different resonance frequencies of the transducer.

transmission line and shielding. The resonance frequency peaks were identified at local minimums of return loss (RL), which is calculated as follows

$$\mathrm{RL} = 10 \log_{10} \frac{P_{\mathrm{rf}}}{P_{\mathrm{in}}} \quad (1)$$

where P_{rf} and P_{in} are the power of reflected and incident signals, respectively.

2.6. Acoustic Power Measurement

Acoustic power was measured with an US power meter UPM-DT-10 (Ohmic Instruments, USA). The device is equipped with a weight sensitive conical target installed inside a water tank (see a scheme in **Figure 4**). The water tank was filled with degassed deionized water until 2 cm gap from the top. The transducer under test was fixed in a custom sample holder. This retainer was positioned on the water surface so that the transducer was centered above the cone-shaped target. The front surface (top electrode) of the transducer was immersed in the water facing down the center of the target, while the back side (PI substrate) was exposed to air. A total of five samples were measured at a selected frequency. The applied voltage and frequency was changed in the working range of the transducer (10–50 MHz) with an arbitrary wave generator connected to the RF amplifier (Hubert A1020, Dr. Hubert GmbH, Germany).

2.7. Pitch and Catch Experiment

Excitation bursts were produced using a waveform generator (33600A Series, Keysight, Santa Rosa, USA), while received signals were obtained using an oscilloscope (InfiniVision MSOX2024A, Keysight, USA). Both transducer devices were connected via coaxial cables to custom-built test benches, which held the transducers at a relative distance of 16 mm. A hydrogel block (Aquaflex, Parker Laboratories, USA) with the same thickness (measured at the time of experiment with a micrometer) and with acoustic properties mimicking human tissue was inserted between the transducers and attached to the test rig. The transducers were excited with a sine wave burst of 4 cycles with frequencies from 5 to 20 MHz at 10 Vpp.

3. Results and Discussion

3.1. Fabrication of the US Transducer

The US transducer was fabricated with a combination of two printing methods—inkjet printing for Ag electrodes and screen printing for P(VDF-TrFE) piezopolymer. The thickness of the printed Ag electrodes was controlled by adjusting the drop spacing. Close control is necessary because changes, especially beyond our suggested thickness, may affect the resonance behavior of the transducers (see Figure S2, Supporting Information). However, the manual screen printing adopted can be accompanied by several technical issues and therefore some special care and strategies have been used. The ink used must not contain any air bubbles, as these can lead to the formation of pinholes in the dry final layer, resulting in short circuits between the Ag electrodes. Air bubbles can be avoided by leaving the ink container in a water ultrasonic bath for at least 30 min. Pinholes and voids between the layers may also occur if the drying temperature is too high. In layer-by-layer printing the liquid layer should not dry too fast in order to let the interface between the layers fuse and form a continuous solid layer. In our case the smooth homogeneous layers were achieved at an optimized $T = 60$ °C. The thickness of the single layer depends on the intrinsic nature of the ink (e.g., viscosity) and printing parameters. Also, the thread mesh count of the silk screen limits the amount of ink that can pass through the mesh. Hence, the average thickness of a single layer of P(VDF-TrFE) with the employed ink and printing setup is ≈2 ± 0.2 µm (mean ± SD), as assessed by means of stylus profilometry measurements.

3.2. Effect of Processing on Ultrasound Transducer

P(VDF-TrFE) crystallizes almost exclusively in the piezoelectric phase similar to β-phase of PVDF.[40] The Curie transition for the P(VDF-TrFE) copolymer with 20 mol % TrFE occurs at T_{Curie} = 136 °C and corresponds to transition from ferroelectric to paraelectric phase.[39] The freshly deposited layers of P(VDF-TrFE) have low crystallinity and therefore must be thermally annealed at a temperature above T_{Curie} but below T_{melt} = 150 °C. Moreover, after thermal annealing the layer consists of randomly oriented polycrystalline piezoelectric domains. A certain electric field has to be applied to align the domains into a single direction (Figure 2a). The field at which the dipoles change their direction is called coercive field (E_c) and in the case of FC20 the coercive field is at E_c = 45 V μm^{-1} (Figure 2b). Thus, for a 12-layer transducer with a total P(VDF-TrFE) thickness of 24 μm, the required polarization voltage must be higher than 1080 V. However, high electric fields during contact polarization can cause mechanical stresses on transducers. Due to the inherent flexibility of polymer substrates, significant deformations can occur during both transient and reverse current flow, hence possibly leading to material breakdown (see Video S1, Supporting Information). To prevent deformation during polarization cycles, we used tape to secure the PI substrates firmly on the working surface. In addition, electrical discharges, especially in the presence of defects or pinholes such as those caused by air pockets or suboptimal temperature treatment (as discussed in previous section), can lead to breakdown of the sample.

During the preliminary optimization of the poling process we observed that the probability of breakdown becomes significant at fields around 100 V μm^{-1} (≈2 * E_c). Therefore, we kept the polarization voltage below this value. The most dramatic evidence of poling is observed in the high-frequency spectrum of the printed transducer before and after poling (Figure 2c). Samples before poling show no clear resonance peaks due to the random orientation of their dipole moments, which causes the net effect of their oscillations to be negligible. By contrast, the poled samples exhibit sharp resonance peaks because all domains are aligned in the same direction, resulting in a stronger and more coherent oscillation. The nature of these peaks will be discussed in the following.

In order to analyze the effect of both processing steps (i.e. the thermal annealing at $T > T_{Curie}$ and the poling at $E > E_C$) we have used XRD and impedance spectroscopy. The piezoelectric phase of P(VDF-TrFE) produces a single diffraction peak in XRD diffractograms at $2\theta = 20°$, corresponding to (100/200) reflection planes.[41] The growth of the peak intensity and decrease of its width is associated with increase of the crystalline content in the deposited layers. Figure 2d shows the XRD of the printed transducer after each processing step. Apart from a clear peak of P(VDF-TrFE) at $2\theta = 20°$, the diffractogram (Figure S3, Supporting Information) also contains broad peaks, which could be attributed to the PI substrate, to Ag nanoparticles from the electrodes of the transducer, and to the Si wafer support. It is evident that the thermal annealing step plays a huge role and increases the peak intensity significantly (by a factor of > 4, FWHM decreases from 0.721° to 0.668°). The subsequent high-voltage poling also improves the crystallinity; however, while the increase of the peak intensity is not so dramatic, the reduction of FWHM (from 0.668° to 0.513°) suggests crystalline domain consolidation into larger crystallites.

Dielectric properties of the P(VDF-TrFE) were studied with impedance spectroscopy. Permittivity is an intrinsic property of a material and does not depend on the thickness. Structural changes which were demonstrated previously with XRD are accompanied with the changes in dielectric permittivity of transducer samples before ("raw") and after annealing and poling (Figure 2e). The low frequency range is associated with the mobility of the dipole moments in the amorphous phase and small crystalline domains. Therefore, the permittivity is high in case of "raw" and "annealed" samples. High voltage poling increases the crystal order and enlarges the size of crystal domains, which leads to reduction of dipole moment and, in turn, of the permittivity (Figure 2e). After both processing steps the permittivity ε' falls in the range ε' = 8–10 at 1 kHz, which perfectly corresponds to the manufacturer's datasheet[39] as well as to values in literature.[41–45]

Hysteresis loops of transducers depict the polarization at the electric field (P–E) and reveal the ferroelectric behavior of the material. Figure 2f shows the typical P–E curve of a poled printed transducer. In such graphs, the intersection with ordinate (both positive and negative) identifies the remnant polarization P_r, while the intersection with abscissa shows the coercive field E_c of the material. The peak in current observed near the maximum electric field indicates the domain switching.[46] The average P_r = 6.39 ± 1.16 μC cm^{-2} is in agreement with figures of merit for other P(VDF-TrFE) transducers given in the literature.[42]

3.3. Characterization of Key Transducer Properties

Our printed US transducer offers several advantageous features that distinguish it from other reported wearable and flexible transducers. These include a low bending radius of ≈3.5 mm,[36] printability, and a compact thickness of ≈75 μm. Table S1 of the Supporting Information provides a summary of these features, as well as additional properties, comparing our printed transducer to other reported wearable and flexible transducers. In addition to material properties discussed so far, the frequency bandwidth and position of resonance peaks, the acoustic power, and the ability to transmit and receive acoustic waves are key characteristics of US transducers.

3.4. Resonance Behavior of Printed US Transducers

In order to accelerate prototyping and facilitate the evaluation of resonance behavior, we employed a previously reported simulation model based on an adapted Mason model and transmission line theory.[36] We validated our simulation results through experimental measurements of printed transducers on a VNA (see details in the Experimental Section).

To identify the substrate allowing the transducer to resonate in the medical bandwidth of interest, we first run simulations using PI substrates with thicknesses of 12.5 and 50 μm. PI films within this thickness are commercially available from various suppliers and therefore constitute feasible substrates. A substrate thickness of 12.5 μm produced a single harmonic at ≈30 MHz (Figure

S4, Supporting Information). However, as the substrate thickness was increased, additional peaks appeared. Figure 3 shows the simulated spectrum of a 24 μm thick P(VDF-TrFE) transducer supported on a 50 μm thick PI substrate. The simulated spectrum shows three resonance–antiresonance pairs of peaks in the studied range. A total of eight transducers with the same dimensions were fabricated and polarized and their frequency spectra were measured. Each spectrum contained the same amount of resonance peaks (f1–f3) and their average position ± standard deviation was superimposed over the simulated spectrum (Figure 3). It is evident that the simulated model predicts the correct positions of the resonances within less than one standard deviation. The deviation from the predicted peak might be caused by the variations in the fabricated transducer due to fabrication with a manual screen printing system. Already the first resonance peak f1 falls into the medical range with the identified resonance at 14.2 ± 0.6 MHz.

3.5. Acoustic Power of the Printed US Transducer

Acoustic power is an important parameter of the US transducer as it determines the intensity of the generated acoustic waves. It is directly proportional to the acoustic pressure directed at a target surface. For medical applications acoustic power is particularly important since it determines the ability of the acoustic waves to penetrate through human tissue. For estimation of acoustic power we have adapted the same ultrasound power meter that is used to measure power output of commercial diagnostic and therapeutic US probes (Figure 4a). The printed US transducer operated in air-backed mode. Due to the acoustic impedances mismatch between PI substrate and air most of the generated acoustic waves are reflected back toward the target, therefore increasing the total acoustic power of the US transducer. Thus, we fabricated a custom sample holder (Figure 4b) that allowed the printed transducer to be stably mounted so that only one face was immersed in the water facing the conical target of the power meter. Figure 4c shows the measured acoustic power of the studied transducer, obtained at three resonant peaks f1–f3. As one face of the sample is immersed in water, the actual resonance peak positions are slightly shifted from the measured values with VNA (Figure 3). The transducer was driven by applying a bipolar voltage through the amplifier (Figure 4a), with the applied voltage varying for each resonant peak. Notably, the peak at f1 = 13.6 MHz required the largest applied voltage, ≈100 V, while the peak at f3 = 42.2 MHz only required 15 V. By applying these voltages, we achieved acoustic power values in the range of several Watts per cm, demonstrating comparable performance to some PZT transducers.[35] As it was shown before, the impedance of the sample decays with increasing frequency, therefore much higher voltages are required for low frequency resonances.

3.6. Pitch and Catch Measurements

The pitch and catch experiments were performed to demonstrate the transmit and receive capabilities of the printed US transducer in the medical ultrasound range. The working frequency was set to 13.7 MHz, which corresponds to the first resonance peak f1 of the sample. In the experimental configuration two printed transducers acted as either transmitter (TX) or receiver (RX). The transmission medium was a 16 mm thick hydrogel block, emulating the properties of human tissues. TX and RX transducers were placed on opposite sides of the hydrogel. The transducers were attached to the hydrogel surface and adhered closely due to the surface tension between the substrate and the moist hydrogel. This adhesion also allowed direct transmission of sound waves through the hydrogel, without further measures, as air was expelled during the deployment of transducers (**Figure 5**). A transmit burst (at 10 Vpp) was sent through TX and the echo was received after 10.2 μs on the RX side. The insertion loss of our transducer was determined at −38 dB and its −6 dB RX bandwidth was at 25% (Figure 5), which aligns well with values reported in the literature.[29] Assuming a speed of sound $v_c = 1570\ \mathrm{ms}^{-1}$ in hydrogel,[47] the travel distance can be calculated and corresponds to the measured thickness of the hydrogel block, confirming the good quality of transduction.

4. Conclusion

The fabrication strategy presented in this paper permitted to realize a fully printed US transducer with tunable resonance properties. The combination of screen and inkjet printing allows the fabrication of transducers with a piezolayer with tunable thickness, with a step of 2 μm per single printed layer in laboratory scale. This cost-effective technology approach is promising for scale-up of production to large volumes, as material costs are low and nonrecurring investments are modest due to the comparably limited complexity of the fabrication process. Moreover, the developed poling process allowed us to achieve high poling fields of ≈100 V μm^{-1}, resulting in high values of Pr (6.39 ± 1.16 μC cm^{-2}). We have identified key parameters that significantly influence the performance of the ultrasound transducer, including the processing of the P(VDF-TrFE) layer and its crystallinity, as well as the thicknesses of the P(VDF-TrFE) layer and the substrate. We have also experimentally confirmed a previously developed open-source simulation model, which will facilitate future developments of the printed US transducers. We demonstrated the operation of the printed US transducer in the medical range with the lowest resonance peak at ≈14 MHz and adapted a commercial power meter to measure the acoustic power of the transducer. We achieved the acoustic power of at least 1 W cm^{-2}, which is comparable to conventional piezoceramic transducers. A pitch and catch experiment performed at this frequency demonstrated the ability of printed US transducers to both transmit and receive the US signal through the human tissue-mimicking hydrogel material. Overall, we believe that these results confirm the potential applicability of the demonstrated printed transducer for medical ultrasound applications such as continuous ultrasound imaging, cardiovascular monitoring, human–machine interfaces, and others.

Supporting Information

Supporting Information is available from the Wiley Online Library or from the author.

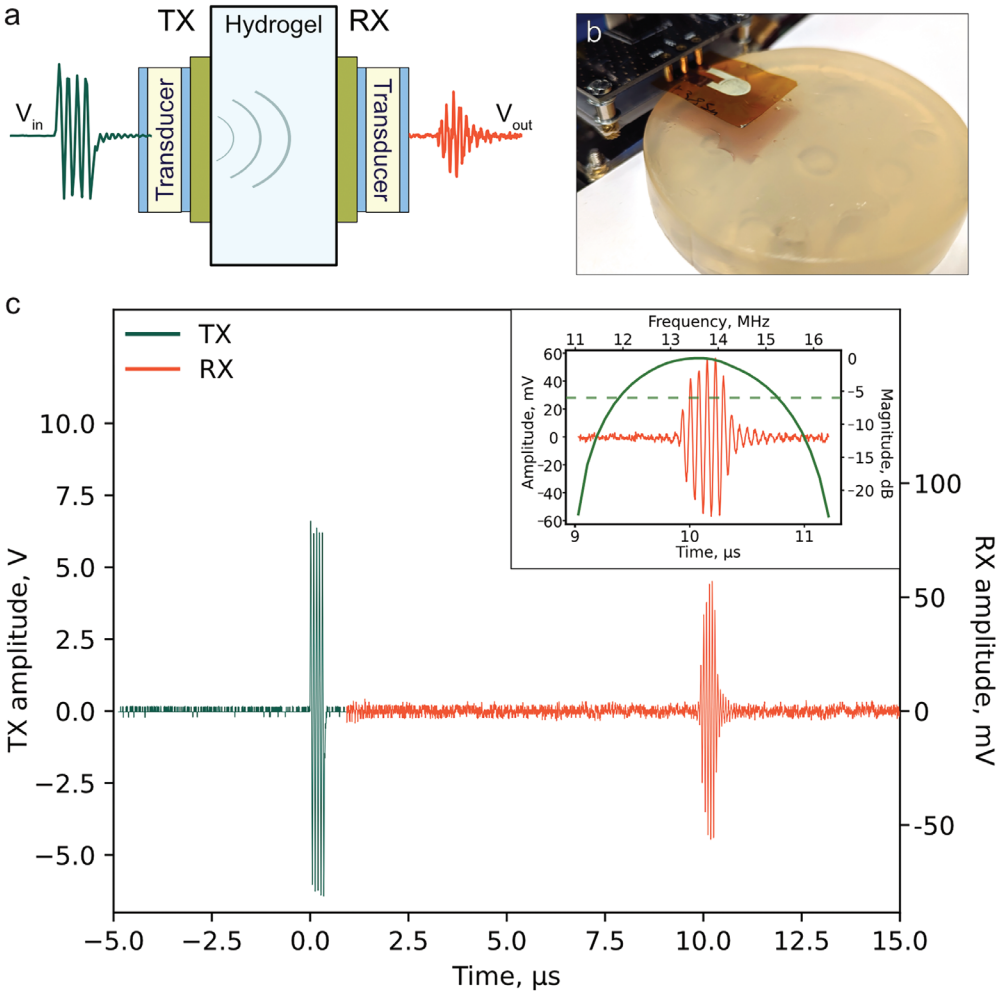

Figure 5. Functionality of the US transducers as transmitter and receiver in pitch and catch experiment: a) illustration of the pitch and catch set-up with two transducers—TX (transmitter) and RX (receiver). b) Photo of one of the printed transducer placed on a hydrogel disk mimicking the properties of human tissue. c) TX pulse and RX amplitudes of the two printed transducers. Inset: the −6 dB bandwidth (dashed green line) of the receiving transducer was from 11.8 to 15.2 MHz (25%).

Acknowledgements

The authors want to thank Prof. Klaus Reichman (TU Graz) for allowing to use the *P–E* hysteresis measurement device in his lab and providing guidance on sample mounting and result interpretation. The authors are grateful to Prof. Roland Resel (TU Graz) for training on XRD diffractometer usage and advice on sample preparation and data analysis. The authors also appreciate Stephan Thurner's contributions to the development of the poling setup and are grateful for his insights and technical support. Moreover, the authors would like to acknowledge Prof. Hermann Scharfetter (TU Graz) for inspiring discussion and technical support of this work. Finally, the authors would like to thank Prof. Joerg Schroettner and Ing. Robert Neubauer of the PMG – European Testing Center of Medical Devices for supporting the acoustic power measurements.

Conflict of Interest

The authors declare no conflict of interest.

Data Availability Statement

The data that support the findings of this study are available from the corresponding author upon reasonable request.

Keywords

piezoelectric, poly(vinylidene fluoride-trifluoroethylene), screen printing, ultrasonic

Received: April 14, 2023
Revised: May 30, 2023
Published online:

[1] P. N. T. Wells, *Phys. Med. Biol.* **2006**, *51*, R83.
[2] J. A. Jensen, *Prog. Biophys. Mol. Biol.* **2007**, *93*, 153.
[3] V. T. Rathod, *Sensors* **2020**, *20*, 4051.

[4] F. Chasset, A. Soria, P. Moguelet, A. Mathian, Y. Auger, C. Francès, S. Barete, *J. Dermatol.* **2016**, *43*, 318.
[5] C. Leitner, P. A. Hager, H. Penasso, M. Tilp, L. Benini, C. Peham, C. Baumgartner, *Sensors* **2019**, *19*, 4316.
[6] S. Vostrikov, A. Cossettini, C. Vogt, C. Leitner, M. Magno, L. Benini, in *2021 IEEE Int. Ultrasonics Symp. (IUS)*, IEEE, Piscataway, NJ **2021**, pp 1–4.
[7] S. Frey, S. Vostrikov, L. Benini, A. Cossettini, in *2022 IEEE Int. Ultrasonics Symp. (IUS)*, IEEE, Piscataway, NJ **2022**, pp. 1–4.
[8] B. Grandi Sgambato, M. Hasbani, D. Y. Barsakcioglu, J. Ibáñez, A. Jakob, M. Fournelle, M.-X. Tang, D. Farina, *High Performance Wearable Ultrasound as a Human Machine Interface for Wrist and Hand Kinematic Tracking*, TechRxiv, IEEE, Piscataway, New Jersey, United States **2023**.
[9] C. Wang, X. Chen, L. Wang, M. Makihata, H.-C. Liu, T. Zhou, X. Zhao, *Science* **2022**, *377*, 517.
[10] C. Wang, B. Qi, M. Lin, Z. Zhang, M. Makihata, B. Liu, S. Zhou, Y. Huang, H. Hu, Y. Gu, Y. Chen, Y. Lei, T. Lee, S. Chien, K.-I. Jang, E. B. Kistler, S. Xu, *Nat. Biomed. Eng.* **2021**, *5*, 749.
[11] H. Hu, H. Huang, M. Li, X. Gao, L. Yin, R. Qi, R. S. Wu, X. Chen, Y. Ma, K. Shi, C. Li, T. M. Maus, B. Huang, C. Lu, M. Lin, S. Zhou, Z. Lou, Y. Gu, Y. Chen, Y. Lei, X. Wang, R. Wang, W. Yue, X. Yang, Y. Bian, J. Mu, G. Park, S. Xiang, S. Cai, P. W. Corey, et al., *Nature* **2023**, *613*, 667.
[12] W. Lee, Y. Roh, *Biomed. Eng. Lett.* **2017**, *7*, 91.
[13] G. de Marzo, V. M. Mastronardi, L. Algieri, F. Vergari, F. Pisano, L. Fachechi, S. Marras, L. Natta, B. Spagnolo, V. Brunetti, F. Rizzi, F. Pisanello, M. De Vittorio, *Adv. Electron. Mater.* **2022**, 2200069.
[14] X. Ma, H. von Seggern, G. M. Sessler, S. Zhukov, O. B. Dali, M. Kupnik, X. Zhang, *Smart Mater. Struct.* **2020**, *30*, 015002.
[15] X. Zhang, X. Zhang, Q. You, G. M. Sessler, *Macromol. Mater. Eng.* **2014**, *299*, 290.
[16] A. Omidvar, E. Cretu, R. Rohling, M. Cresswell, A. J. Hodgson, *Adv. Mater. Technol.* **2023**, *8*, 2201316.
[17] C. D. Gerardo, E. Cretu, R. Rohling, *Microsyst. Nanoeng.* **2018**, *4*, 1.
[18] F. Merbeler, S. Wismath, M. Haubold, C. Bretthauer, M. Kupnik, *Micromachines* **2022**, *13*, 676.
[19] B. Stadlober, M. Zirkl, M. Irimia-Vladu, *Chem. Soc. Rev.* **2019**, *48*, 1787.
[20] N. Izyumskaya, Y.-I. Alivov, S.-J. Cho, H. Morkoç, H. Lee, Y.-S. Kang, *Crit. Rev. Solid State Mater. Sci.* **2007**, *32*, 111.
[21] P. E. Bloomfield, W.-J. Lo, P. A. Lewin, *IEEE Trans. Sonics Ultrason.* **2000**, *47*, 1397.
[22] F. S. Foster, K. A. Harasiewicz, M. D. A Sherar, *IEEE Trans. Sonics Ultrason.* **2000**, *47*, 1363.
[23] W. D. Middleton, A. B. Kurtz, B. S. Hertzberg, *Ultrasound: The Requisites*, Mosby, Amsterdam, Netherlands **2004**.
[24] R. Dallaev, T. Pisarenko, D. Sobola, F. Orudzhev, S. Ramazanov, T. Trčka, *Polymers* **2022**, *14*, 4793.
[25] S. Mohammadpourfazeli, S. Arash, A. Ansari, S. Yang, K. Mallick, R. Bagherzadeh, *RSC Adv.* **2023**, *13*, 370.
[26] H. Yuan, T. Lei, Y. Qin, R. Yang, *Nano Energy* **2019**, *59*, 84.
[27] U. Pierre Claver, G. Zhao, *Adv. Eng. Mater.* **2021**, *23*, 2001187.
[28] V. T. Rathod, D. R. Mahapatra, A. Jain, A. Gayathri, *Sens. Actuators, A* **2010**, *163*, 164.
[29] L. F. Brown, *IEEE Trans. Sonics Ultrason.* **2000**, *47*, 1377.
[30] H. Li, Y. Ma, Y. Huang, *Mater. Horiz.* **2021**, *8*, 383.
[31] S. Sherrit, *Characterization of Piezoelectric Materials for Transducers*, p. 45, https://doi.org/10.48550/arXiv.0711.2657.
[32] T. E. G. Alvarez-Arenas, *IEEE Trans. Sonics Ultrason.* **2004**, *51*, 624.
[33] I. Al Mohimeed, M. Agarwal, Y. Ono, in *2018 IEEE Canadian Conf. on Electrical and Computer Engineering (CCECE)*, IEEE, Quebec City, QC **2018**, pp. 1–4.
[34] S. Wagle, A. Decharat, P. Bodö, F. Melandsø, *Appl. Phys. Lett.* **2013**, *103*, 262902.
[35] N. R. Harris, M. Hill, R. Torah, R. Townsend, S. Beeby, N. M. White, J. Ding, *Sens. Actuators, A* **2006**, *132*, 311.
[36] C. Leitner, K. Keller, S. Thurner, C. Baumgartner, F. Greco, H. Scharfetter, J. Schröttner, in *2022 IEEE Int. Symp. on Applications of Ferroelectrics (ISAF)*, IEEE, Piscataway, NJ **2022**, pp. 1–4.
[37] C. K. McGinn, K. A. Kam, M.-M. Laurila, K. Lozano Montero, M. Mäntysalo, D. Lupo, *J. Appl. Phys.* **2020**, *128*, 225304.
[38] Piezoelectricity in polymers: Critical reviews in solid state and materials sciences: Vol 9, No 4, https://www.tandfonline.com (accessed: March **2023**).
[39] Piezoelectric materials P(VDF-TRFE) Arkema Piezotech, https://piezotech.arkema.com/en/Products/piezoelectric-copolymers/(accessed: March **2023**).
[40] N. Shingne, *Ph.D. Thesis*, University of Halle, Germany, **2011**.
[41] R. I. Mahdi, W. C. Gan, W. H. A. Majid, *Sensors* **2014**, *14*, 19115.
[42] D. Thuau, K. Kallitsis, F. D. D. Santos, G. Hadziioannou, *J. Mater. Chem. C* **2017**, *5*, 9963.
[43] J. Li, Q. Meng, W. Li, Z. Zhang, *J. Appl. Polym. Sci.* **2011**, *122*, 1659.
[44] V. Sencadas, C. M. Costa, V. Moreira, J. Monteiro, S. K. Mendiratta, J. F. Mano, S. Lanceros-Méndez, *e-Polymers* **2005**, *5*.
[45] Q. Liu, M. Q. Le, C. Richard, R. Liang, P.-J. Cottinet, J.-F. Capsal, *Org. Electron.* **2019**, *67*, 259.
[46] A. Kumar, V. V. Bhanu Prasad, K. C. James Raju, A. R. James, *J. Mater. Sci.: Mater. Electron.* **2015**, *26*, 3757.
[47] A. F. Prokop, S. Vaezy, M. L. Noble, P. J. Kaczkowski, R. W. Martin, L. A. Crum, *Ultrasound Med. Biol.* **2003**, *29*, 1351.